IEEE Access
Multidisciplinary | Rapid Review | Open Access Journal

Received July 18, 2019, accepted July 29, 2019, date of publication August 9, 2019, date of current version September 5, 2019.

Digital Object Identifier 10.1109/ACCESS.2019.2934112

Wideband Tightly Coupled Dipole Arrays With Balanced Scattering and Radiation Based on a Black-Box Method

ZHECHEN ZHANG, SHIWEN YANG, (Senior Member, IEEE), JIANHUI HUANG, SHIWEI XIAO, YIKAI CHEN, (Senior Member, IEEE), AND SHIWEI QU, (Senior Member, IEEE)

School of Electronic Science and Engineering, University of Electronic Science and Technology of China, Chengdu 611731, China

Corresponding authors: Shiwen Yang (swnyang@uestc.edu.cn) and Yikai Chen (ykchen@uestc.edu.cn)

This work was supported by the National Natural Science Foundation of China under Grant 61631006, Grant 61571101, and Grant 61721001.

ABSTRACT A key challenge in the new generation of advanced phased arrays is to realize wideband and wide-scanning performances while maintaining lower scattering characteristics. In this paper, a black box method (BBM) is proposed for accelerating balanced optimization of radiation and monostatic scattering characteristics of an antenna element in an infinite periodic environment. To validate the method, a common tightly coupled dipole array (TCDA) with unbalanced feed scheme is considered. Besides, the indium tin oxide (ITO) film is introduced to further improve the wide-angle scanning and monostatic scattering reduction abilities. Finally, a 10×10 single-polarized TCDA prototype with ITO film is fabricated and measured. Measured results are in good agreement with simulation results and demonstrate that the TCDA has a balanced radiation and scattering characteristics, such as an active VSWR < 3.0 over $7 - 18$ GHz while scanning up to 60° in E-/H-plane and a broadband monostatic scattering reduction.

INDEX TERMS Phased array, tightly coupled dipole array, black box method (BBM), antenna scattering.

I. INTRODUCTION

Wideband phased arrays are developing rapidly in order to support next generation communication and electronics applications. Traditional Vivaldi array models and technologies have been widely used to achieve wide bandwidth and wide-angle beam scanning [1]–[4]. In spite of their desirable impedance bandwidth, the antenna profiles of Vivaldi arrays are usually rather high, which lead to higher cross-polarization and are difficult for conformal applications.

The tightly coupled dipole arrays (TCDAs) utilize their capacitive coupling between the adjacent elements to cancel the inductive load resulting from the short-circuited ground plane effects. Owing to their obvious advantages such as low profile, ultra-wide bandwidth, and wide-angle beam scanning, many innovative studies on such kind of array have been proposed in the past decades [5]–[8]. To achieve very wide bandwidth, the dipoles of TCDAs are usually fed by Marchand baluns [9]–[12] or 50Ω twin coaxial feed lines [13], and resistive sheets used to prevent the array from being shorted are implemented to the TCDAs. Nevertheless, it is necessary to weld the junction between the dipole and the balun, and vertical baluns may introduce an extra scattering source. In order to reduce the profile height of the arrays and make them much more integrated and easier to assemble, planar ultra-wideband modular antenna (PUMA) arrays were proposed [14]. The arrays consist of tightly coupled dipoles printed on grounded dielectric substrates, and each of the dipoles is fed directly from a 50Ω unbalanced interface, using a pair of shorting posts placed on the opposite sides of arms to shift off the common-mode resonance. In this circumstance, the entire array is able to be optimized altogether instead of designing arrays and baluns separately. Moreover, traditional analytical methodologies for wideband arrays such as the Green's functions [15]–[20] and the equivalent circuit methods for TCDAs [21]–[22] are merely suitable for simplified antenna structures, and the cases for oblique incidences are rarely taken into account yet.

On the other hand, modern advanced electronic platforms not only put forward the requirements of phased arrays with

The associate editor coordinating the review of this article and approving it for publication was Lu Guo.

wide-angle scanning performance over a broadband, but also take the low scattering of the entire array systems into consideration. However, the studies on the in-band scattering reduction of TCDAs have been rarely presented. Most of the studies on monostatic scattering reduction of antennas focused on simple micro-strip patch antennas [23]–[25]. Among these strategies, the artificial periodic structures are mounted on the same plane as the radiating patch to reduce the dominant scattering contributed by the grounds. In [26], a method of using polarization conversion metamaterial [27] was proposed to obtain the reduction of RCS. However, the cases for small incidence angles were only considered, and in order to preserve radiation characteristics, the in-band RCS has not been suppressed.

When receiving antenna is well matched, this situation may still happen where the receiving antenna can not absorb all the EM waves. The purpose of this paper is to further reduce the scattering of antenna with minimum sacrifice of radiation performance. In this paper, a 10 × 10 single-polarized TCDA operating over 6–18 GHz is designed and the balance of radiation and in-band scattering performances is simultaneously realized for the first time. In an attempt to satisfy these requirements, a black box method (BBM) is proposed for the fast analysis TCDA elements within infinite arrays [28], where the entire antenna element is regarded as a two-port network, and the radiation and scattering of TCDA can be optimized efficiently. It is worth to be mentioned that the BBM is a general analysis method without bandwidth limitation for unknown two-port network, especially for the cases where equivalent circuit model of the network is difficult to be obtained. Furthermore, indium tin oxide (ITO) film is adopted as a wide-angle impedance matching (WAIM) layer for the first time to realize wide-angle beam scanning and lower monostatic scattering simultaneously, without sacrificing the antenna gains obviously.

This paper is organized as follows. Section II shows the design process of the TCDA antenna elements in detail. The numerical approach BBM and ITO film are described in detail. Section III presents the fabrication of prototype array optimized by BBM. The measurement results of radiation and scattering characteristics are given and the effectiveness of method is illustrated. Finally, conclusions are drawn in Section IV.

II. THE PROCESS OF ANTENNA ELEMENT DESIGN BASED ON BBM

The most critical aspect in this design of TCDA is the BBM as it helps realize the fast balanced optimization of radiation and monostatic scattering characteristics. The brief description about the geometry of the original TCDA element is given for completeness. As shown in Fig. 1, the radiation dipoles end-terminated with interdigital capacitor are printed on top of a Taconic TLY-5 substrate dielectric layer 1, with permittivity and thickness to be $\varepsilon_{r1} = 2.2$ and $h_1 = 1mm$, respectively. The dielectric layer 3 ($\varepsilon_{r3} = 2.2$ and $h_3 = 3.175mm$) is served as a supporting layer, which guarantees the structural robustness of the array. Dielectric layers 1 and 3 are laminated together with dielectric layer 2 a piece of prepreg ($\varepsilon_{r2} = 2.81$ and $h_2 = 0.122mm$). To mitigate the scan blindness [20], perforations are drilled throughout the stackup. Underneath the dipole arms, small rectangular patches are used to increase the capacitive coupling. As shown in Fig. 1(c), the inner conductor of a 50Ω coaxial connector passes through a hole in the aluminum plate ($h_5 = 2mm$), acting as an impedance transformer. The dielectric layer 4 ($\varepsilon_{r4} = 2.2$ and $h_4 = 2mm$) serves as a WAIM layer which can be used to improve the scanning performance. Finally, four asymmetric shorting posts are adopted in the present model to move the common-mode resonance to higher frequency. As compared to the structure of dual symmetric shorting posts in [29], numerical results show that the structure of four asymmetric shorting posts is more robust and effective for removing the common-mode resonance within an ultra-wideband.

A. BLACK BOX METHOD (BBM)

In this subsection, the BBM is proposed to simplify the equivalent circuit model of TCDA. To allow the readers to understand the function of BBM easily, the process of designing proposed TCDA unite cell is presented in the following:

1) The original TCDA with only a thin dielectric layer is designed firstly. The simulated VSWR is shown in Fig. 3.
2) A black box method (BBM) is proposed to extract the ABCD matrix of original TCDA unite cell without WAIMs.
3) The equivalent circuit model is adopted to fast optimize and balance the characteristics of radiation and scattering using PSO optimization algorithm.
4) The indium tin oxide (ITO) film optimized is covered on the surface of TCDA to attain wide-angle scanning and good scattering characteristics.

As shown in Fig. 2, the WAIMs on top of the antenna are normally equivalent to transmission lines [30]–[31]. Based on the use of BBM, the complicated equivalent lumped elements of TCDA without WAIMs can be simplified into a two-port network just like a black box. Then, the input impedance looking into the excited port of antenna can be expressed as

$$Z_{in} = \frac{AZ_L + B}{CZ_L + D} \tag{1}$$

which is equivalent to

$$Z_L A + B - Z_L Z_{in} C - Z_{in} D = 0 \tag{2}$$

In order to extract ABCD matrix of the equivalent two-port network of the original TCDA without WAIMs, the parameters of antenna keep unchanged. Simultaneously, a fixed layer (Rogers 5880, $h_1 = 1$mm) and a variable layer above are used to ensure that the network is not interfered by the newly added WAIMs to some degree. By changing the thickness of the variable layer, three samples of input impedance $<Z_{in}, Z_L>$ can be obtained, and the normalized ABCD matrix is then calculated by solving the homogeneous linear equations.

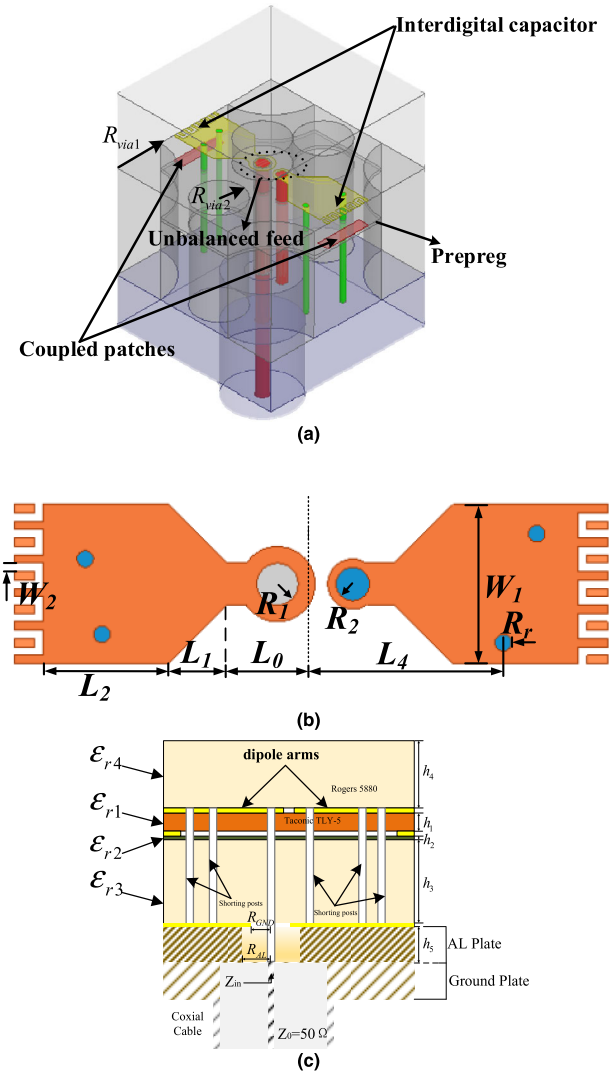

FIGURE 1. 6-18 GHz single-polarized modified TCDA elements. (a) 3D graphic of a typical TCDA element. (b) Top view of dipole layer. (c) Front view of the entire element. Some optimized key parameters (length in mm) are: $R_r = 0.1$, $L_0 = 1$, $L_1 = 0.7$, $L_2 = 1.5$, $L_3 = 0.25$, $W_1 = 1.7$, $W_2 = 0.1$.

Generally, three samples are needed in order to extract the intrinsic two-port network parameters for a specific scan angle, given by

$$\begin{bmatrix} Z_{L1} & 1 & -Z_{L1}Z_{in1} & -Z_{in1} \\ Z_{L2} & 1 & -Z_{L2}Z_{in2} & -Z_{in2} \\ Z_{L3} & 1 & -Z_{L3}Z_{in3} & -Z_{in3} \end{bmatrix} \begin{bmatrix} A \\ B \\ C \\ D \end{bmatrix} = \begin{bmatrix} 0 \\ 0 \\ 0 \end{bmatrix} \tag{3}$$

where the leftmost matrix is regarded as $\hat{A}$, and let $[A, B, C, D]^T$ be X for the sake of convenience. As for the homogeneous linear equation $\hat{A}X = 0$, the solution vector is the eigenvector corresponding to the minimum eigenvalue of matrix $\hat{A}^*\hat{A}$.

According to the substrate equivalent transmission line theory, for a substrate with thickness d, its ABCD matrix is given by

$$\begin{bmatrix} A & B \\ C & D \end{bmatrix} = \begin{bmatrix} \cos(k_i d) & jZ_{diel}^{TE/TM} \sin(k_i d) \\ jY_{diel}^{TE/TM} \sin(k_i d) & \cos(k_i d) \end{bmatrix} \tag{4}$$

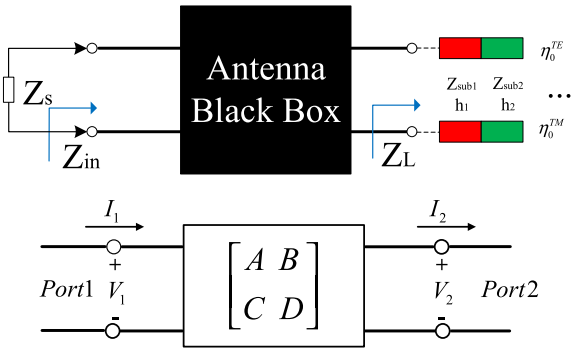

FIGURE 2. Equivalent two-port network for one TCDA element.

As shown in Fig. 2, the infinite free space is equivalent as a resistance. However, when the electromagnetic wave is obliquely incident, the equivalent characteristic impedance of substrate will be changed [10]. As shown in (8) and (9), the equivalent impedance varies with the incident angle θ, given by

$$Z_{diel}^{TE} = \frac{\eta_0}{\sqrt{\varepsilon_r - \sin^2\theta}} \tag{5}$$

$$Z_{diel}^{TM} = \frac{\eta_0\sqrt{\varepsilon_r - \sin^2\theta}}{\varepsilon_r} \tag{6}$$

According to the definition of scattering, the scattering cross-section is given by

$$\sigma = \lim_{R\to\infty} 4\pi R^2 \frac{|E_s|^2}{|E_i|^2} \tag{7}$$

where E_s and E_i are the scattering and incident electric field. When a plane wave perpendicularly incident to the surface of the TCDA element, the strength of reflected power E_s is decided by the surface reflection coefficient. Thus, it implies that it is able to reduce the monostatic scattering through the optimization of the surface reflectance, provided that the array is infinite and there is no edge diffraction.

The surface impedance of the infinite antenna element can be extracted by using commercial software HFSS simulation where master/slave boundary and Floquet port excitation are used. Then, the antenna array in the receiving mode can be considered as an absorber. When efforts are made to match the absorber to the free space by optimizing the WAIMs which means that the surface reflection coefficient is optimized to be smaller enough for incident wave, the scattering of antenna is reduced. Simultaneously, the wide-angle beam scanning performance is also able to be improved by optimizing the WAIM parameters. Therefore, the equivalent circuit model based on BBM in Fig. 2 can be applied in the balanced optimization of radiation performance and monostatic scattering characteristic programmatically.

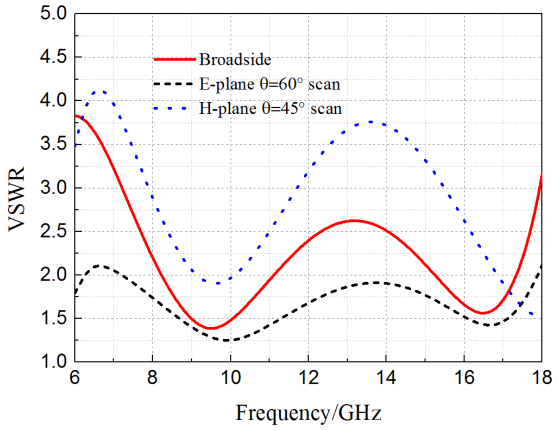

FIGURE 3. Active VSWR of the unoptimized TCDA element under beam scan condition.

Fig. 3 shows the scanning VSWR of the TCDA element with a fixed thin layer. It is observed that the result is barely satisfactory and the WAIMs of antenna still need to be further optimized. Consequently, particle swarm optimization (PSO) algorithm is adopted.

Here, a global optimization algorithm PSO algorithm [32] is utilized to search the optimal permittivity and thickness of the dielectrics. Suppose that the number of the dielectric layers is N, then the optimization parameters can be written as a vector denoted as:

$$X_i = [\varepsilon_{r1}, \varepsilon_{r2}, \ldots \varepsilon_{rN}, H_1, H_2, \ldots H_N]^T \tag{8}$$

where the subscripts are arranged from top to bottom of the dielectric layers.

The variations of these optimization parameters during the iteration process satisfy the following rules:

$$\begin{aligned} V_{k+1}(j) &= w \cdot V_k(j) + c_1 \cdot r_1 \cdot [X_k(jbest) - X_k(j)] \\ &\quad + c_2 \cdot r_2 \cdot [X_k(elite) - X_k(j)] \end{aligned} \tag{9}$$

$$X_{k+1}(j) = X_k(j) + V_{k+1}(j) \tag{10}$$

where $V_k(j)$ and $X_k(j)$ represent the velocity and value of the particle j in the kth iteration. $X_k(jbest)$ is the best particle in kth iteration, and $X_k(elite)$ is the elite particle number in the swarm until kth iteration. r_1 and r_2 in (12) are random real-numbers ranging from 0 to 1. Cognitive parameter c_1, social parameter c_2, and the inertia weight w are the fundamental algorithm parameters of PSO. Here, c_1 and c_2 both are selected as 1.5, and $w = 1$.

Additionally, a swarm with 20 particles is used to search for the optimal solution through 100 optimization iterations. Considering that the profile of the antenna should be as low as possible, the upper bound of the permittivity and thickness are selected as 3.5 and 1mm, while the lower bound of them are selected as 1.5 and 0.5mm respectively. Then, the particle swarm is initialized and the proposed method is adopted to calculate the active VSWR while adding dielectric layers ($N = 3$). To realize the balance of radiation and scattering performance, the fitness function is given as:

$$fitness = 0.5 \times fitness_{VSWR} + 0.5 \times fitness_{scat} \tag{11}$$

$$\begin{aligned} fitness_{VSWR} = 0.25 \times & \left. \frac{\sum_{i=1}^{k} fitness_{VSWR}(i)}{k} \right|_{broadband} \\ & + 0.25 \times \left. \frac{\sum_{i=1}^{k} fitness_{VSWR}(i)}{k} \right|_{E60^\circ} \\ & + 0.5 \times \left. \frac{\sum_{i=1}^{k} fitness_{VSWR}(i)}{k} \right|_{H45^\circ} \end{aligned} \tag{12}$$

$$fitness_{scat} = \frac{\sum_{i=1}^{k} fitness_{scat}(i)}{k} \tag{13}$$

$$fitness_{VSWR}(i) = \begin{cases} 0 & if\ VSWR(i) \le value1(i) \\ VSWR(i) & \\ \quad - value1(i) & if\ VSWR(i) > value1(i) \end{cases} \tag{14}$$

$$fitness_{scat}(i) = \begin{cases} 0 & if\ reflect(i) \le value2(i) \\ reflect(i) & \\ \quad - value2(i) & if\ reflect(i) > value2(i) \end{cases} \tag{15}$$

In (14)-(18), $fitness_{VSWR}$ and $fitness_{scat}$ are the fitness functions for the active VSWR of beam scanning and the fitness function for surface reflection coefficient, respectively. In this process, three typical VSWR performances (namely, the broadside, 60° scan in E-plane and 45° scan in H-plane) are taken into consideration. k is the number of frequency points, and i is the sequential number of specific frequency point. The threshold of $value1(i)$ is set to 2 for all frequencies, and $value2(i)$ is set to -15 (dB) within 8-12GHz and -10 (dB) in other frequency bands, respectively.

Fig. 4(a) shows the convergence curve of optimization obtained after about 60 iterations. The final optimized results vector is $X = [2.2, 1.7, 1.5, 1, 1, 1]^T$. As can be seen from Fig. 4(b), it is observed that the calculation based on our equivalent two-port network model and the results simulated by HFSS are in good agreement for both broadside state and beam scanning states. Fig. 4(c) presents the comparison of surface reflection coefficient. It is shown that the optimized result has considerable back-scattering reduction as compared to the original one, and there is about 10dB reduction at 17GHz. The monostatic scattering result comparison between the original and optimized TCDA is presented in Fig. 4 (d). According to Fig. 4, numerical results verify that BBM performs well in improving the active VSWR and reducing monostatic scattering of the TCDA simultaneously.

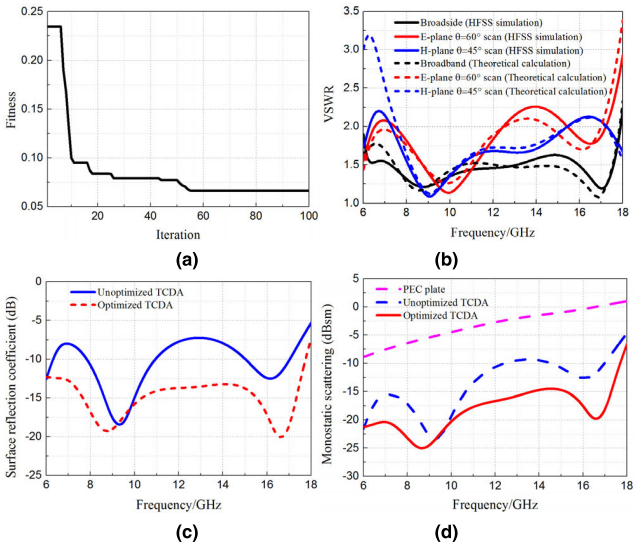

FIGURE 4. Optimized results for TCDA in an infinite array. (a) Fitness curve for PSO optimization. (b) Simulated VSWR versus frequency and scan angle. (c) Surface reflection coefficients for unoptimized TCDA and optimized TCDA. (d) Monostatic scattering comparison of the unoptimized TCDA and optimized TCDA forming a 10 × 10 array.

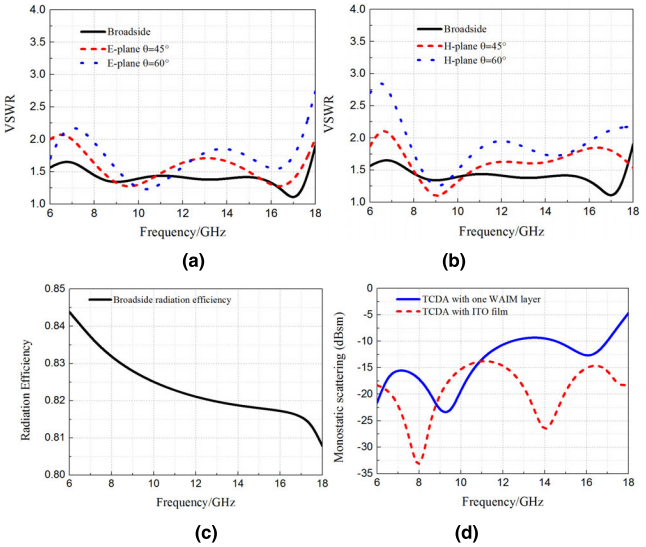

FIGURE 6. The radiation and scattering performance of the TCDA element in in an infinite array. (a) Active VSWR vs. frequency in E-plane scan. (b) Active VSWR vs. frequency in H-plane scan. (c) Broadband radiation efficiency for TCDA with ITO layer. (d) Monostatic scattering of 10 × 10 TCDA with one WAIM layer and an ITO film.

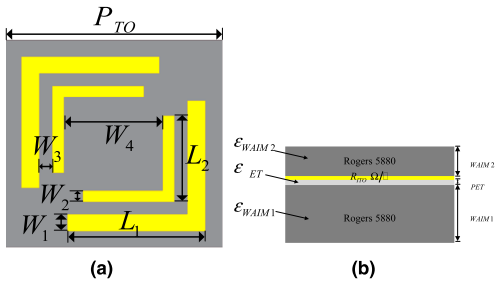

FIGURE 5. Layouts of the WAIM layers upon the surface of TCDA. (a) Top view of the ITO layer and its structural parameters. (b) Front view of the entire WAIM layers. Optimized key parameters (length in mm) are: $W_1 = 0.7$, $W_2 = 0.3$, $W_3 = 0.2$, $W_4 = 2.8$, $L_1 = 4$, $L_2 = 2.5$, $P_{ITO} = 7.1$, $R_{ITO} = 300\Omega$/sq.

B. ITO BASED WAIM LAYER

As mentioned before, the thickness and permittivity of the WAIM layers can be optimized programmatically based on the aforementioned theory. However, it is still inefficient to optimize the WAIM layers within a low profile limitation, due to the thickness of WAIM layers will increase in the case of large scanning angles. According to Fig. 2, if a proper impedance is paralleled in front of the free space, the high resistance level posing the challenge when matching to standard 50Ω interfaces will be declined. With regard to back-scattering reduction, it has been validated that reducing the surface reflection is equivalent to the reduction of monostatic scattering. Inspired from [33], the indium tin oxide (ITO) film is innovatively implemented as a WAIM layer placed upon TCDA to help realize the balanced optimization of scanning radiation performances and the reduction of monostatic scattering, simultaneously.

In the process of optimizing the ITO layer, the TCDA unite cell with dielectric layers remains the same ($\varepsilon_{WAIM1} = 2.2$, $\varepsilon_{WAIM2} = 2.2$, $H_{WAIM1} = 2mm$, $H_{WAIM1} = 1mm$). The WAIM layout is depicted in Fig. 5, where it can be seen that the ITO film with a thickness of a few nanometers is etched on a thin PET substrate.

The unit-cell simulations with periodic boundary conditions on all walls are carried out with a PML absorbing layer terminated at the top of the unit cell. The simulation results are shown in Fig. 6. The active VSWR for scanning in the E-plane is substantially less than 2.0, with a maximum of 3.0 near 18 GHz. There is a hump of 3.0 near 6GHz in the H-plane 60° scanning. Fig. 6(c) displays the broadband radiation efficiency for the TCDA with ITO film. The result over the entire frequency band is between 0.8 and 0.85, which is still good as compared to the results in [13]. Fig.6(d) shows the comparison of scattering of TCDA with and without one ITO film while maintaining other structure and materials unchanged. Overall, this modified TCDA is able to realize a 60° 2D scanning in 3:1 bandwidth and keeps a dramatic reduction of monostatic scattering simultaneously, meanwhile preserves high radiation efficiency.

III. FABRICATION AND MEASUREMENT RESULTS

As shown in Fig. 7 the 10 × 10 TCDA prototype with ITO film is divided into several parts to fabricate and assemble. Specifically, the laminate, ITO films, dielectric WAIMs, aluminum plate and ground plate are fabricated individually. Ultimately, they are fixed together by inserting four plastic screws into holes at the edge of each part, and the size of the entire array is 71mm × 71mm.

The S-parameters of the single-polarized 10 × 10 prototype were measured by using a vector network analyzer.

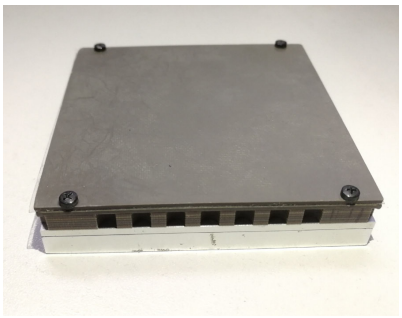

FIGURE 7. Overall view of the assembled 10 × 10 single-polarized TCDA.

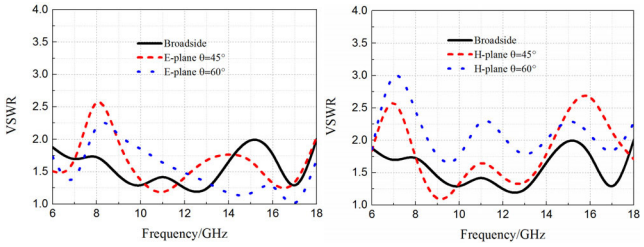

FIGURE 8. Simulated active VSWR of one central element in the 10 × 10 finite TCDA. (a) E-plane scan; (b) H-plane scan.

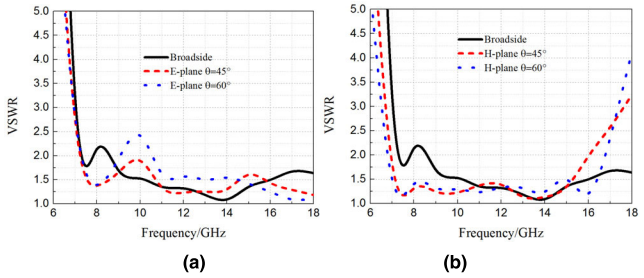

FIGURE 9. Measured active VSWRs of a central element in 10 × 10 TCDA. (a) E-plane scan. (b) H-plane scan.

The active reflection coefficient of an element $(p,\ q)$ can be calculated from

$$\Gamma_{pq}(\theta, \varphi) = \sum_{m=1}^{M} \sum_{n=1}^{N} S_{mn,pq} e^{-j([m-p]D_x u + [n-q]D_y v)} \qquad (16)$$

where (θ, φ) is the array scan direction; $u = ksin\theta cos\varphi$ and $v = ksin\theta sin\varphi$ are the u-v coordinates; k is the wavenumber in the free-space, $S_{mn,pq}$ represents the measured isolation between elements $(m,\ n)$ and $(p,\ q)$. M, N and D_x, D_y are the index numbers of elements and element spacing along the x and y dimensions, respectively.

The simulated active VSWR versus frequency for broadside and E-/H-plane scan are shown in Fig. 8. Simulated results show good impedance matching performance. However, deterioration usually emerges on smaller finite arrays as compared to infinite array predictions [17]. Measured active VSWRs of a central element are shown in Fig. 9 for broadside, $\theta = 45°$ and $g\theta = 60°$ scan in the E- and H-planes.

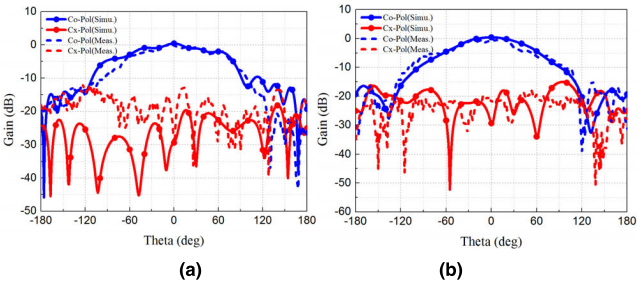

FIGURE 10. Measured and simulated central port element patterns of the single-polarized 10 × 10 TCDA at 13GHz. (a) E-plane. (b) H-plane.

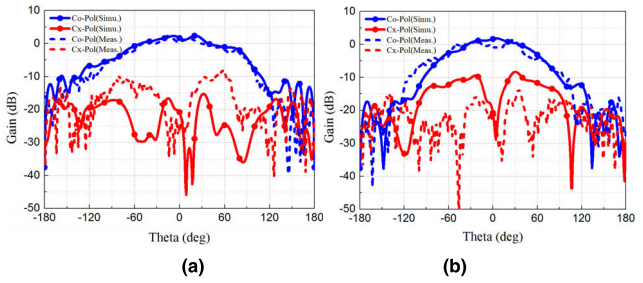

FIGURE 11. Measured and simulated central port element patterns of the single-polarized 10 × 10 TCDA at 16GHz. (a) E-plane. (b) H-plane.

The results reveal that the VSWR in 6-7GHz band has some degradation, due to that the array guided surface waves (AGSWs) are excited at the finite array edges, especially considering that the center element is only about $0.6\lambda_{low}$ apart from the array edges. Moreover, the assembly error also results in some phase errors during the measurement. However, AGSWs are not the focus of this work. In practical applications, larger arrays may alleviate the deterioration of VSWR at lower frequency [34]. The measurement was carried out at the ports of SMP-SMA adapter cables, and the VSWR data has been compensated by taking into account the insertion loss of the cables. It is noted that for beam scanning, the reflections from the elements are not in-phase, hence the reflected power is inevitably absorbed within the cables, resulting in artificially lower measured VSWR, especially for beam scanning in H-plane.

The embedded element pattern is a good way to indicate the scanning performance in a large array [35]. The far-field pattern measurements are conducted in an anechoic chamber. A wideband ridged horn antenna operating over 1-18GHz is used for transmitting antenna and three standard gain horn antennas are used as calibration. E-/H-plane realized gain patterns for central element at 13GHz and 16GHz are shown in Fig. 10 and Fig. 11 respectively. Measurements and finite array simulations are in good agreement for all cases, with some differences in the cross-polarization.

Fig. 12 and Fig. 13 show the measured and simulated E-/H-plane scan patterns at 13GHz and 16GHz, respectively. It is observed that beam pointing and gain level for broadside and scan cases are in very good agreement. While scanning up to a larger angle, the main beam deviates slightly

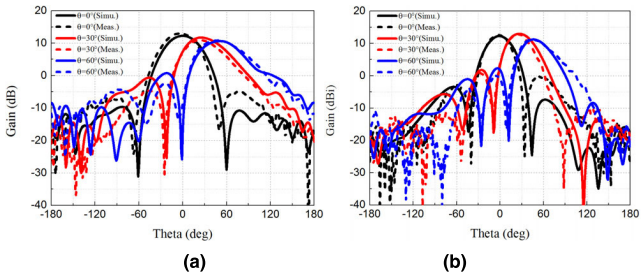

FIGURE 12. Measured and simulated co-polarized patterns of the single-polarized 10 × 10 TCDA in the E-/H- plane (13GHz). (a) E-plane scan. (b) H-plane scan.

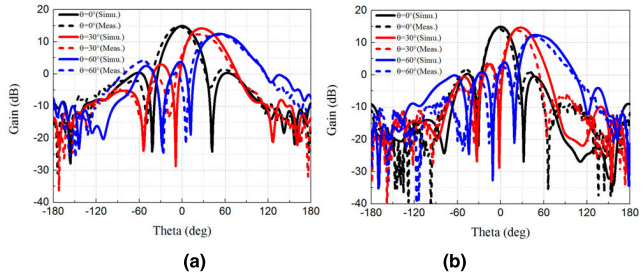

FIGURE 13. Measured and simulated co-polarized patterns of the single-polarized 10 × 10 TCDA in the E-/H- plane (16GHz). (a) E-plane scan. (b) H-plane scan.

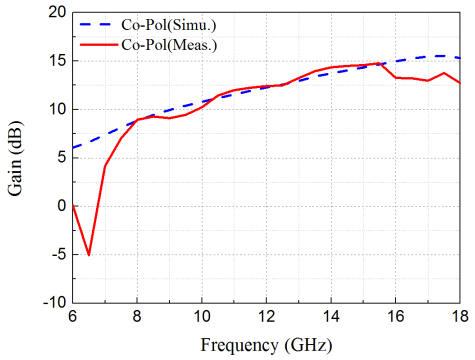

FIGURE 14. Measured and simulated broadside realized gain for the 10 × 10 single-polarized TCDA.

from the desired direction as a result of the rather smaller size of the prototype array.

The comparison between measured and simulated broadside co-polarized gain versus frequency of the prototype array is plotted in Fig. 14. It can be observed that the co-polarized gain closely tracks the simulated one to within 1 dB across the frequency band of 8.0-15.5GHz. The fluctuations above and below the simulated gain curve are ascribed to the electrically small size of prototype array ($\lambda_{low} = 50$mm), which is susceptible to AGSWs. The destructive active VSWR in 6-7GHz band causes the deterioration of measured gain. As for the higher frequency, the sideband (16-18GHz) effect of the transmitting horn antenna has affected the accuracy of the measured results. Besides, fabrication tolerance may also result in some discrepancy.

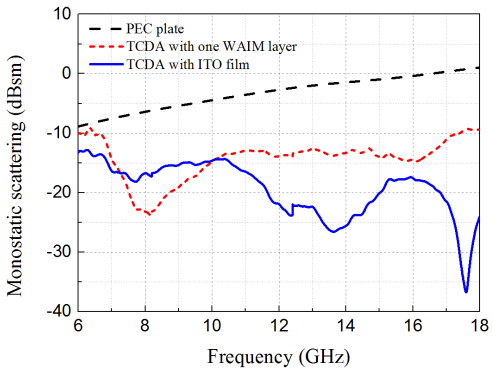

FIGURE 15. Monostatic scattering comparison between the results of the TCDA with ITO film and those of the TCDA with one WAIM layer.

For the purpose of verifying the monostatic scattering reduction performance of the proposed single-polarized TCDA, the monostatic scattering under normal incidence with co-polarized wave of the prototype with ITO film and the prototype with one WAIM layer were measured respectively. Fig. 15 gives the comparison of the measured monostatic scattering results of the 2 prototypes, indicating that TCDA with ITO film has a significant scattering reduction over majority of the operation bandwidth. A maximum reduction of 25dB is achieved at 17.5GHz. The existence of AGSWs in such a smaller finite array leads to a little deterioration at the lower frequency band. The fabrication and assembly process may also introduce some unknowns bringing about the frequency shift. Additionally, the antenna array may not be strictly aligned with the test system for a few degrees of deviation, since that it is too difficult to adjust the TCDA antenna precisely vertical to the reflector antenna and horizontal to the ground during the measurement, thus leading to some uncontrollable effects on the monostatic scattering measurements.

IV. CONCLUSION

This paper presents the detailed theory, design, fabrication and measurement of a TCDA with wideband, wide scanning and reduced monostatic scattering characteristics. A black-box method is proposed to realize the balanced optimization of radiation performance and monostatic scattering characteristics simultaneously. By implementing an ITO film as one of the WAIM layers, the monostatic scattering can be further reduced while maintaining wide-angle beam scanning performance within wide bandwidth. A single-polarized 10 × 10 TCDA operating over 6-18GHz was designed and measured. Measured results verified the good radiation and scattering performance of the designed TCDA. The proposed BBM and the ITO film provide an effective way of designing a wideband and wide-scan TCDA with lower monostatic scattering. Although only monostatic RCS of proposed antenna is reduced in this paper, the control of scattering performance under oblique incidence can also be realized based on the proposed method.

REFERENCES

[1] N. Schuneman, J. Irion, and R. Hodges, "Decade bandwidth tapered notch antenna array element," in *Proc. Antenna Appl. Symp.*, Sep. 2001, pp. 283–294.

[2] J. D. S. Langley, P. S. Hall, and P. Newham, "Balanced antipodal Vivaldi antenna for wide bandwidth phased arrays," *IEE Proc. Microw., Antennas Propag.*, vol. 143, no. 2, pp. 97–102, Apr. 1996.

[3] T.-H. Chio and D. H. Schaubert, "Parameter study and design of wide-band widescan dual-polarized tapered slot antenna arrays," *IEEE Trans. Antennas Propag.*, vol. 48, no. 6, pp. 879–886, Jun. 2000.

[4] D. H. Schaubert, S. Kasturi, A. O. Boryssenko, and W. M. Elsallal, "Vivaldi antenna arrays for wide bandwidth and electronic scanning," in *Proc. 2nd Eur. Conf. Antennas Propag. (EuCAP)*, Nov. 2007, pp. 1–6.

[5] Y. Zhou, F. Zhu, S. Gao, Q. Luo, L.-H. Wen, Q. Wang, X. Yang, Y. Geng, and Z. Cheng, "Tightly coupled array antennas for ultra-wideband wireless systems," *IEEE Access*, vol. 6, pp. 61851–61866, 2018.

[6] L. Zhang, S. Gao, Q. Luo, W. Li, Y. He, and Q. Li, "A wideband circularly polarized tightly coupled array," *IEEE Trans. Antennas Propag.*, vol. 66, no. 11, pp. 6382–6387, Nov. 2018.

[7] H. Zhang, S. Yang, Y. Chen, J. Guo, and Z. Nie, "Wideband dual-polarized linear array of tightly coupled elements," *IEEE Trans. Antennas Propag.*, vol. 66, no. 1, pp. 476–480, Jan. 2018.

[8] S. Xiao, S. Yang, Y. Chen, S.-W. Qu, and J. Hu, "An ultra-wideband tightly coupled dipole array co-designed with low scattering characteristics," *IEEE Trans. Antennas Propag.*, vol. 67, no. 1, pp. 676–680, Jan. 2019.

[9] E. Yetisir, N. Ghalichechian, and J. L. Volakis, "Ultrawideband array with 70° scanning using FSS superstrate," *IEEE Trans. Antennas Propag.*, vol. 64, no. 10, pp. 4256–4265, Oct. 2016.

[10] J. P. Doane, K. Sertel, and J. L. Volakis, "A wideband, wide scanning tightly coupled dipole array with integrated balun (TCDA-IB)," *IEEE Trans. Antennas Propag.*, vol. 61, no. 9, pp. 4538–4548, Sep. 2013.

[11] W. F. Moulder, K. Sertel, and J. L. Volakis, "Ultrawideband superstrate-enhanced substrate-loaded array with integrated feed," *IEEE Trans. Antennas Propag.*, vol. 61, no. 11, pp. 5802–5807, Nov. 2013.

[12] M. H. Novak and J. L. Volakis, "Ultrawideband antennas for multiband satellite communications at UHF–Ku frequencies," *IEEE Trans. Antennas Propag.*, vol. 63, no. 4, pp. 1334–1341, Apr. 2015.

[13] W. F. Moulder, K. Sertel, and J. L. Volakis, "Superstrate-enhanced ultrawideband tightly coupled array with resistive FSS," *IEEE Trans. Antennas Propag.*, vol. 60, no. 9, pp. 4166–4172, Sep. 2012.

[14] S. S. Holland and M. N. Vouvakis, "The planar ultrawideband modular antenna (PUMA) array," *IEEE Trans. Antennas Propag.*, vol. 60, no. 1, pp. 130–140, Jan. 2012.

[15] A. Neto and J. J. Lee, "'Infinite bandwidth' long slot array antenna," *IEEE Antennas Wireless Propag. Lett.*, vol. 4, pp. 75–78, 2005.

[16] D. Cavallo, A. Neto, and G. Gerini, "Analytical description and design of printed dipole arrays for wideband wide-scan applications," *IEEE Trans. Antennas Propag.*, vol. 60, no. 12, pp. 6027–6031, Dec. 2012.

[17] A. Neto, D. Cavallo, and G. Gerini, "Edge-born waves in connected arrays: A finite × infinite analytical representation," *IEEE Trans. Antennas Propag.*, vol. 59, no. 10, pp. 3646–3657, Oct. 2011.

[18] A. Neto, D. Cavallo, G. Gerini, and G. Toso, "Scanning performances of wideband connected arrays in the presence of a backing reflector," *IEEE Trans. Antennas Propag.*, vol. 57, no. 10, pp. 3092–3102, Oct. 2009.

[19] A. Neto and S. Maci, "Green's function for an infinite slot printed between two homogeneous dielectrics. I. Magnetic currents," *IEEE Trans. Antennas Propag.*, vol. 51, no. 7, pp. 1572–1581, Jul. 2003.

[20] D. Cavallo, W. H. Syed, and A. Neto, "Equivalent transmission line models for the analysis of edge effects in finite connected and tightly coupled arrays," *IEEE Trans. Antennas Propag.*, vol. 65, no. 4, pp. 1788–1796, Apr. 2017.

[21] E. A. Alwan, K. Sertel, and J. L. Volakis, "Circuit model based optimization of ultra-wideband arrays," in *Proc. IEEE IEEE Int. Symp. Antennas Propag.*, Jul. 2012, pp. 1–2.

[22] B. Riviere, H. Jeuland, and S. Bolioli, "New equivalent circuit model for a broadband optimization of dipole arrays," *IEEE Antennas Wireless Propag. Lett.*, vol. 13, pp. 1300–1304, 2014.

[23] Y. Zhao, X. Cao, J. Gao, X. Yao, T. Liu, W. Li, and S. Li, "Broadband low-RCS metasurface and its application on antenna," *IEEE Trans. Antennas Propag.*, vol. 64, no. 7, pp. 2954–2962, Jul. 2016.

[24] Y. Liu and X. Zhao, "Perfect absorber metamaterial for designing low-RCS patch antenna," *IEEE Antennas Wireless Propag. Lett.*, vol. 13, pp. 1473–1476, 2014.

[25] P. Mei, X. Q. Lin, J. W. Yu, and P. C. Zhang, "A band-notched absorber designed with high notch-band-edge selectivity," *IEEE Trans. Antennas Propag.*, vol. 65, no. 7, pp. 3560–3567, Jul. 2017.

[26] S. Xiao, S. Yang, H. Zhang, H. Bao, Y. Chen, and S.-W. Qu, "A low-profile wideband tightly coupled dipole array with reduced scattering using polarization conversion metamaterial," *IEEE Trans. Antennas Propag.*, to be published.

[27] Y. Jia, Y. Liu, Y. J. Guo, K. Li, and S.-X. Gong, "Broadband polarization rotation reflective surfaces and their applications to rcs reduction," *IEEE Trans. Antennas Propag.*, vol. 64, no. 1, pp. 179–188, Jan. 2016.

[28] J. Huang, S. Yang, Y. Chen, and S. Qu, "Black box method for the radiation and scattering optimization of TCDA," in *Proc. IEEE Asia–Pacific Conf. Antennas Propag.*, Aug. 2018, pp. 87–88.

[29] S. S. Holland, D. H. Schaubert, and M. N. Vouvakis, "A 7–21 GHz dual-polarized planar ultrawideband modular antenna (PUMA) array," *IEEE Trans. Antennas Propag.*, vol. 60, no. 10, pp. 4589–4600, Oct. 2012.

[30] X. Begaud, F. Linot, M. Soiron, and C. Renard, "Analytical model of a self-complementary connected antenna array on high impedance surface," *Appl. Phys. A, Solids Surf.*, vol. 115, no. 2, pp. 517–522, May 2014.

[31] S. Varault, M. Soiron, A. Barka, A. C. Lepage, and X. Begaud, "RCS reduction with a dual polarized self-complementary connected array antenna," *IEEE Trans. Antennas Propag.*, vol. 65, no. 2, pp. 567–575, Feb. 2017.

[32] L. Lizzi, F. Viani, R. Azaro, and A. Massa, "A PSO-driven spline-based shaping approach for ultrawideband (UWB) antenna synthesis," *IEEE Trans. Antennas Propag.*, vol. 56, no. 8, pp. 2613–2621, Aug. 2008.

[33] O. Hashimoto, T. Abe, Y. Hashimoto, T. Tanaka, and K. Ishino, "Realisation of resistive-sheet type wave absorber in 60 GHz frequency band," *Electron. Lett.*, vol. 30, no. 8, pp. 657–658, Apr. 1994.

[34] H. Holter and H. Steyskal, "On the size requirement for finite phased-array models," *IEEE Trans. Antennas Propag.*, vol. 50, no. 6, pp. 836–840, Jun. 2002.

[35] D. M. Pozar, "The active element pattern," *IEEE Trans. Antennas Propag.*, vol. 42, no. 8, pp. 1176–1178, Aug. 1994.

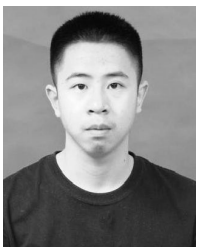

ZHECHEN ZHANG was born in Shaowu, Fujian, China, in 1996. He received the B.S. degree in electromagnetic field and wireless technology from the University of Electronic Science and Technology of China, Chengdu, China, in 2018, where he is currently pursuing the Ph.D. degree in electromagnetics and microwave technology.

His current research interests include UWB antenna arrays, phased arrays, and low scattering antennas and arrays.

SHIWEN YANG (M'00–SM'04) was born in Langzhong, Sichuan, China, in 1967. He received the B.S. degree in electronic science and technology from East China Normal University, Shanghai, China, in 1989, and the M.S. degree in electromagnetics and microwave technology and the Ph.D. degree in physical electronics from the University of Electronic Science and Technology of China (UESTC), Chengdu, China, in 1992 and 1998, respectively.

From 1994 to 1998, he was a Lecturer with the Institute of High Energy Electronics, UESTC. From 1998 to 2001, he was a Research Fellow with the School of Electrical and Electronic Engineering, Nanyang Technological University, Singapore. From 2002 to 2005, he was a Research Scientist with Temasek Laboratories, National University of Singapore, Singapore. Since 2005, he has been a Full Professor with the School of Electronic Engineering, UESTC. He has been a Chang-Jiang Professor nominated by the Ministry of Education of China, since 2015. He has authored or coauthored over 300 technical papers. His current research interests include antennas, antenna arrays, optimization techniques, and computational electromagnetics.

Prof. Yang was a recipient of the Foundation for China Distinguished Young Investigator presented by the National Natural Science Foundation of China, in 2011. He is currently the Chair of the IEEE Chengdu AP/EMC Joint Chapter and serves as an Editorial Board Member for the *International Journal of Antennas and Propagation* and the *Chinese Journal of Electronics*.

JIANHUI HUANG was born in Hengyang, Hunan, China, in 1994. He received the B.S. degree in electromagnetic field and wireless technology, in 2015, and the M.S. degree in electromagnetics and microwave technology from the University of Electronic Science and Technology of China (UESTC), Chengdu, China, in 2019.

His current research interests include UWB antenna arrays, phased arrays, and low scattering antennas and arrays.

SHIWEI XIAO was born in Dazhou, Sichuan, China, in 1992. He received the B.S. degree in electromagnetic field and wireless technology from the University of Electronic Science and Technology of China, Chengdu, China, in 2015, where he is currently pursuing the Ph.D. degree in electromagnetics and microwave technology.

His current research interests include UWB antenna arrays, phased arrays, and low scattering antennas and arrays.

YIKAI CHEN was born in Hangzhou, China, in 1984. He received the B.Eng. and Ph.D. degrees in electromagnetics and microwave technology from the University of Electronic Science and Technology of China (UESTC), Chengdu, China, in 2006 and 2011, respectively.

From 2011 to 2015, he was a Research Scientist with Temasek Laboratories, National University of Singapore, Singapore. In 2015, he joined UESTC, as a Full Professor. He has authored or coauthored over 100 peer-reviewed papers and 25 patents/patent disclosures. He has coauthored the book entitled *Characteristic Modes: Theory and Applications in Antenna Engineering* (John Wiley, 2015), and one book chapter to *Differential Evolution: Fundamentals and Applications in Electrical Engineering* (IEEE-Wiley, 2009). His current research interests include antenna engineering, computational electromagnetics, and evolutionary optimization algorithms in electromagnetic engineering.

Dr. Chen is a member of the Applied Computational Electromagnetics Society (ACES). He was a recipient of the National Excellent Doctoral Dissertation Award of China, in 2013. He was recognized as a Hundred Talents Program Professor of the UESTC, a Thousand Talents Program Professor of China, and a Thousand Talents Program Professor of Sichuan Province, China, in 2015, 2016, and 2017, respectively. He served many international conferences as a TPC Member, a Session Organizer, and a Session Chair. He serves on an Editorial Board for the *Chinese Journal of Electronics*, and the Review Boards of 11 journals.

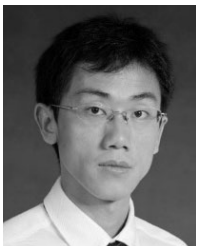

SHIWEI QU (S'08–M'11–SM'12) was born in China, in 1980. He received the B.Eng. and M.Sc. degrees from the University of Electronic Science and Technology of China (UESTC), Chengdu, China, in 2001 and 2006, respectively, and the Ph.D. degree from the City University of Hong Kong (CityU), Hong Kong, in 2009. He was with the Tenth Institute of Chinese Information Industry, Taiwan, from 2001 to 2002. He was a Research Assistant with the Department of Electronic Engineering, CityU, from 2006 to 2007. He was a COE (Global Center of Excellence) Research Fellow and a Postdoctoral Fellow with Tohoku University, Sendai, Japan, from 2009 to 2010. He is currently an External Member of the State Key Laboratory of Millimeter Waves, Partner Laboratory, CityU, and also a Full Professor with the School of Electronic Engineering, UESTC. He has authored or coauthored over 70 internationally refereed papers and over 50 international conference papers. His current research interests include UWB antennas and arrays, phased arrays, and millimeter-wave/terahertz antennas and arrays.